Shearing stellar interferometer. 1: Digital data analysis scheme

Erez Ribak and Elia Leibowitz

A method to extract the visibility of celestial objects in real time using a parallel-shear interferometer is described. Such an instrument produces fringes of constant visibility but with random atmospheric-induced phases. The fringes are modulated internally, and synchronuous detection with many parallel channels recovers their contrast. First, we perform parallel sine and cosine phase-locked accumulation for the short period in which the atmosphere is presumed frozen. The visibility amplitude is then calculated allowing for Poisson noise. We find that a 7.8^m star can be resolved by a single detector to the diffraction limit of the telescope; with twenty such detectors, the limit is 10^m.

I. Introduction

Amplitude interferometry and speckle interferometry are two competing methods in high resolution astronomy. Speckle interferometry is a relatively new and more successful technique being simpler to apply (but longer to reduce the acquired data). Amplitude interferometry has had less trials, because of more complicated instrumentation, but has now revived, because of new optical and detecting techniques. At the same time speckle methods reverted to more advanced optical and detection schemes, thus making it comparable to amplitude interferometry. The main reasons to favor amplitude interferometry are a (theoretical) higher SNR for brighter objects and a simpler way to obtain real-time results.

There exists a variety of amplitude interferometers. They can be classified into either single or multi-telescope systems as well as into image or aperture interferometers. The latter can be sorted into rotating, folding, variable, or parallel (lateral) shear. This paper refers mainly to the last type. The results, however, apply to other shearing interferometers.

The following sections will describe the principle behind the lateral-shear interferometer and the reasons behind its choice. The signal detection scheme devised for it will be analyzed, and an effort will be made to estimate its capabilities. A separate paper[1] will describe the instrument.

II. Principle

In this section we will describe the principle behind the parallel-shear interferometer. A general background of the subject is given in optics books[2,3] and in review articles specifically concerning high resolution interferometry.[4–9]

Amplitude interferometry consists of measuring the mutual coherence function formed by a stellar object at a telescope aperture. The intensity at the exit pupil of the interferometer will be a result of interference of the images of the telescope aperture:

$$I = I_1 + I_2 + 2(I_1 I_2)^{1/2}|g_{12}| \cos(\phi + \theta), \tag{1}$$

where I_1 and I_2 are the intensities at the two images, and ϕ is the phase of the coherence function g_{12}. θ is the phase difference between the two paths and is caused by optical and atmospheric aberrations. The fringe visibility in the interference pattern is

$$V = \frac{I_{\max} - I_{\min}}{I_{\max} + I_{\min}} = \frac{2|g_{12}|}{(I_1/I_2)^{1/2} + (I_2/I_1)^{1/2}}. \tag{2}$$

Although others[10,11] have proposed methods for estimating $|g_{12}|$, we apply a digital photon counting approach to the measurement of the coherence function. Since the phase of the fringes is not known, their intensity is measured at four phases, 90° apart, and these provide a basis for another estimator of $|g_{12}|^2$. The details are given later.

Intensity interferometers were built over the years[4,12–16] followed by shearing interferometers.[17–24] The difference between the two kinds is in the measurement plane: the first at the stellar image, the second in the aperture plane. The main problem

The authors are with Tel Aviv University, Physics & Astronomy Department, Ramat Aviv, Tel Aviv 69978, Israel.

Received 27 October 1984.
0003-6935/85/183088-06$02.00/0.

plagueing virtually all these interferometers was their poor detection system. As the atmosphere corrugates the incoming wave front, the interference fringe pattern is strongly influenced. One is limited, therefore, to detect with many independent detectors for short integration times only. Single photomultipliers are quite inefficient, as is the human eye or a photographic film. Their limited bandwidth—temporal, spatial, or both—makes them inadequate for this purpose.

It can be shown[11] that the number of independent detectors has to be at least four times the number of isoplanatic patches to be able to sample the fringes above the Nyquist limit set by the atmosphere. An alternative scheme is to introduce internal fringe phase modulation (by changing the relative path length between the interfering rays). This moves each fringe across a single detector rather than having the four detectors look at different parts of the fringe. A drawback of this scheme is the limited efficiency of most modulation methods. Linear path changes limit strongly the light bandwidth, while sinusoidal path changes lead to a nonsinusoidal fringe movement. For the latter case, the fringe intensity will behave like

$$I(t) = I_1 + I_2 + 2(I_1 I_2)^{1/2} |g_{12}| \cos(\phi + k \cos t), \qquad (3)$$

where k is the amplitude of the modulation. We can choose such a value for k so as to make the right-hand term nearly harmonic with a maximum amplitude of 0.7.

The system described here utilizes a parallel-shear interferometer.[23] In this kind of interferometer all interference points correspond to the same separation between entrance points. This separation (or shear) can also be identified with a particular spatial frequency. As the mutual coherence is position-independent and is a function only of separation, the fringe visibility should be the same for all points except for the atmospheric-induced phase. If a bank of detectors measures the fringe amplitude, all results should be the same. These amplitudes are then added incoherently, averaging over space and time. This way the mutual coherence of the object can be determined for one spatial frequency. To obtain the 2-D coherence function, the value of shear is changed from zero to the telescope radius and its direction over 180°.

Folding and rotational shear, in contrast with parallel shear, have the advantage of giving directly the 1- or 2-D coherence function. However, because most telescopes have a central obscuration, a complementary parallel shear is usually required to get the low spatial frequencies. At the same time, each detector looks at a particular spatial frequency making it impossible to average over many detectors. Therefore, averaging must be performed over time only, and particular spatial frequencies cannot be singled out for longer measurement, as is the case with lateral shear.

Another difference between the methods is the number of detectors required to recover the available information. In parallel-shear interferometers only a limited number of detectors is needed along the (varying) overlap area of the apertures. In rotational shear the overlap area is constant and maximal, thus saving on light. However, this requires many more detectors, since their output cannot be averaged.

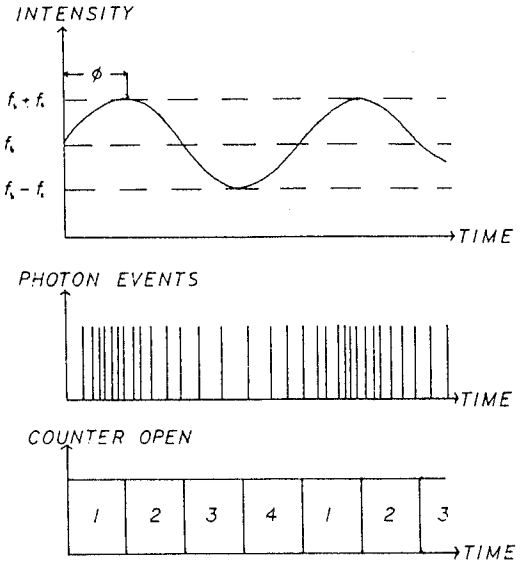

Fig. 1. Modulated signal entering the detector (top) and after the amplifier (center). Each counter collects pulses for one quarter of a cycle (bottom).

Thus it seems that the best solution might be an amalgam of instruments and detection techniques. One hopes that next generation optics and detectors will make it possible to attain the potential that theory predicts for amplitude interferometers.[9]

III. Signal Processing

This section describes the signal handling which was adopted in this work. It applies directly to the parallel-shear interferometer but can be adopted easily for any other kind. Briefly, it consists of finding the photon structure function of the interference pattern at one frequency only.[25,26] Since the atmosphere-induced phase fluctuations have random amplitudes and random temporal frequency, it is much easier to utilize instead internal modulation. Digital synchronuous methods are used to single out only the component at this modulation frequency eliminating all other frequencies (including the constant background).

Let a single detector look at an area smaller than one-half of the fringe spacing. As a first approximation, we assume that the fringe phase is constant over this area; later we will consider the degradation of the signal due to the finite detector size. Properly aligned, the fringe spacing is set to infinity. Under atmospheric turbulence it will decrease, so that there is no point in adjusting the fringe spacing much above the size of the isoplanatic patch. The average input to a detector of area A will be proportional to the instantaneous intensity (Fig. 1):

$$f(t) = \frac{1}{A} \iint_A d^2\mathbf{r} \left[U(\mathbf{r},t) + V(\mathbf{r},t) \cos\left(\frac{2\pi t}{T} + \phi \right) \right], \qquad (4)$$

where U is the background flux, V is the modulation

signal, and ϕ is the combined phase of the coherence function and the atmospheric-induced path difference. T is the modulation cycle time.

Since the background and modulated signal are independent, we employ a standard demodulation scheme (a lock-in amplifier) to find the signal. This signal is then compared to the background to find the modulation depth. The whole demodulation is carried out in a digital manner and is analyzed accordingly. The lock-in amplification technique is the standard method used for finding the amplitude and phase of a small alternating signal of known frequency bathed in a high background. This is done by singling out a Fourier harmonic: the signal and background are multiplied by the cosine of the modulation frequency and integrated for as long as possible (say T_1). Specifically

$$f_C = \int_0^{T_1} dt f(t) \cos \frac{2\pi t}{T} = V \cos\phi. \tag{5}$$

If we could integrate for infinite time, we would get the exact harmonic. Thanks to the atmosphere, the phase of the signal is changing every so often, and T_1 is rather limited. Thus we do not have an infinitely narrow bandwidth but a finite one.

In digital phase-sensitive detection Eq. (5) is realized by entering the train of pulses representing the detected signal into an up–down counter, the latter flipping at the modulation frequency. During the first half-cycle the counter accumulates the pulses. It then flips and counts them backward, subtracting from the previous sum and turning negative if necessary. By the next switching, that is, after a full period, it continues counting up again. After an integration time T_1 the result is read from this counter. If we enter the pulses simultaneously into another up–down counter set up to flip in quadrature with the former one, we will get a corresponding sine term. Squaring and adding these two terms should give the squared amplitude of the signal independent of the random phase. The same procedure is repeated for many T_1 periods and over many parallel channels so as to get a proper average of the squared amplitude.

To find the required amplitude, we have to calculate the expectation value and variance of these estimators for the sine and cosine terms as well as for the squared amplitude. Assume for simplicity that we direct the pulses from the detector into four counters, each collecting for a quarter of a period and then cycling back to the first one (Fig. 2). By summing and subtracting these four counters, we can reproduce the sine and cosine up–down counters. The number of counts at the jth counter ($j = 1, \ldots, 4$) after K_1 cycles, or after a total time of $T_1 = K_1 T$, is

$$p_j = \frac{T}{4} \sum_{i=1}^{K_1} U_{ij} + V_{ij}\sqrt{2} \int_\phi^{T_1} dt \frac{1}{A} \iint_A d^2\mathbf{r} \cos[\phi(\mathbf{r},t) + \pi j/2]. \tag{6}$$

To find the expected values of these quantities, we assume that they obey Poisson statistics. If so, they can be separated into additive terms with additive expected

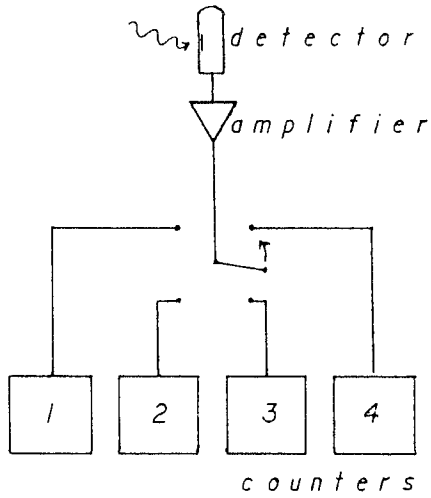

Fig. 2. Cyclic channeling of photon pulses into four counters.

values. The terms are a constant background flux and a time-varying signal flux. It is convenient to separate further the latter into a product of some constant (signal) flux and a harmonic factor. We substitute for the time average background flux $U = \langle U_{ij} \rangle$ for the time average signal flux $V = \langle V_{ij} \rangle$ (both over T_1) and $\langle \cos(\phi + \pi j/2) \rangle$ as the time–area average of the cosine term. In case the fringe spacing is infinite and their phase is continuous (no atmospheric disturbance), the latter is just the mathematical average. Otherwise the random effect must be accounted for (see below). The expected value of P_j is thus

$$s_j = \langle p_j \rangle = \frac{T_1}{4} [U + \sqrt{2} V \langle \cos(\phi + \pi j/2) \rangle]. \tag{7}$$

The four counters serve as building blocks and can be combined in different manners (Fig. 3). In the lock-in detection method described above, we form a cosine term by subtraction of the accumulations from two adjacent counters from the other two and likewise for a sine. Another combination, much simpler to implement and calculate, is to form the cosine term by subtracting the contents of the third counter from the first and ignore the other two. The sine would use the second and fourth counters and ignore the first and third. This way no two counters will be active at the same time, and the covariance of the sine and cosine will be zero. Later, we will require the total flux falling on the detector. For that, we will add the contents of the four counters.

The following step is to square the sine and cosine terms and add them so as to get an estimate of the signal squared amplitude. This is done K_2 times for a (second) integration time $T_2 = K_2 T_1$. We form the estimators

$$S_0 = \sum_{k=1}^{K_2} (p_{1k} - p_{3k})^2 + (p_{2k} - p_{4k})^2, \tag{8}$$

$$N_0 = \sum_{k=1}^{K_2} p_{1k} + p_{2k} + p_{3k} + p_{4k}. \tag{9}$$

The second estimator serves to measure the total amount of light that was collected during the acquisi-

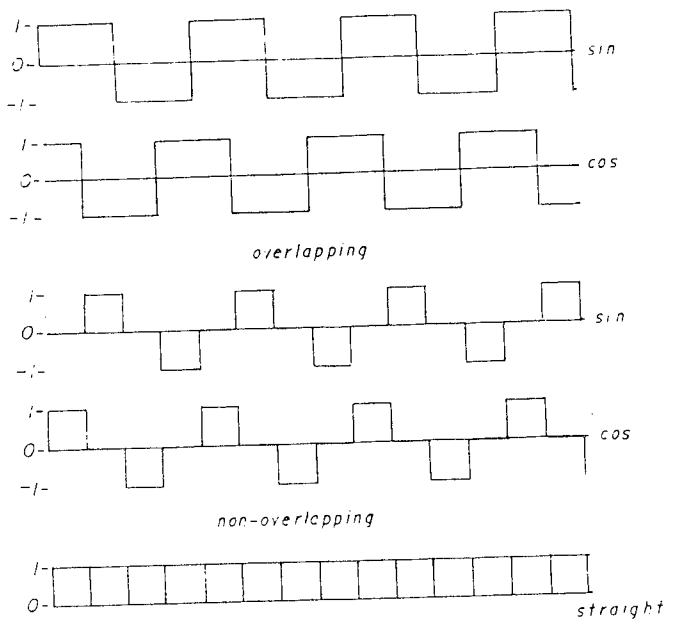

Fig. 3. Schemes to achieve sine and cosine approximations by adding and subtracting every two of the four (quarter cycle) counters for each (top) or by adding and subtracting every second one (center). The straight counter adds them all up (bottom).

tion. The expectation values and variances of these estimators are calculated in the Appendix. The straight flux counter N_0 gives

$$N = E(N_0) = \mathrm{var}(N_0) = T_2U, \tag{10}$$

while the squared-and-added sine–cosine term expectation value and variance are

$$S = E(S_0) = N(1 + Wm^2/2), \tag{11}$$

$$\mathrm{var}(S_0) = N(1 + W + 2Wm^2 + W^2m^2), \tag{12}$$

where $W = T_1U = N/K_2$ is the average flux during the short integration, and m is the sought modulation term:

$$m = (V/U)(\langle\sin\phi\rangle^2 + \langle\cos\phi\rangle^2)^{1/2}. \tag{13}$$

When atmospheric effects are negligible, the sine–cosine term on the right is close to unity. The effect of this assumption is that the time–area average means constancy of phase during the short exposure time T_1 as well as over a single detector. If one is not satisfied with this assumption, the sine–cosine term will have to be measured using a known object (e.g., a point source). Theoretical estimates also exist.[27]

We are trying to measure the fringe visibility, namely, the ratio V/U, which appears in the expression for m. Since S_0 is a biased estimator of m^2, we form another estimator:

$$P_0 = 2K_2\frac{S_0 - N_0 - 2}{N_0^2}. \tag{14}$$

The choice of this expression was made under the requirements that the bias and variance of m^2 will be minimal. Expending P_0 in a Taylor series around S_0 and N_0, we find

$$P = E(P_0) = m^2\left(1 + \frac{3}{N}\right) - \frac{12K_2}{N^3} = m^2\left(1 + \frac{3}{N}\right) - \frac{12}{NW^2}, \tag{15}$$

$$\mathrm{var}(P_0) = \frac{4K_2[2K_2 + N(1 + 4m^2)]}{N^3} + \frac{12}{N}$$

$$= \frac{4[2 + W(1 + 4m^2)]}{NW^2} + \frac{12}{N}, \tag{16}$$

where we have neglected higher-order terms in $1/W$. This is permitted for $W > 1$ or for more than one photon per short integration time T_1. At lower fluxes we can still use this estimator, but both the bias and variance will be more appreciable. Thus it seems that P_0 is a good estimator for m^2 and is adopted from now on.

We know that our background is not solely contributed by the starlight interfering with itself. Other sources might be sky background, detector dark current, light scattered within the system, or simply light from a nonoverlapping (and thus noninterfering) area. Careful engineering and good observing conditions will eliminate most of these sources, but even with their presence not all is lost. Their inclusion contradicts our assumption that the modulation depth is equal to the contrast, and we must calibrate this background level. We can measure the modulation depth of a strong point source where the contrast should always be unity and the SNR high. We then divide the measured modulation depth from any extended source by that of the point source, yielding the real contrast of the former. If the calibration point source produces a clear smooth signal, the noise introduced by this division is negligible. Assuming that the two measurements were done under similar atmospheric conditions, the degradation in the sine–cosine square term [in the estimate for m, Eq. (13)] will be the same for each spatial frequency, and the division of the two measurements will eliminate it.

We now estimate the limiting stellar magnitude for which resolvable objects can be measured with this system. We assume that atmospheric conditions let us integrate coherently for $T_2 = 2$ msec. If we want to map the 2-D coherence function of an object and a reference star in one night, we will use for our object ~7 h and measure it in four orientations, 45° apart, each at 32 shear points. (The reference star can be measured for one orientation only.) The accumulation time for each shear point will be about $T_2 = 200$ sec, which makes $K_2 = T_2/T_1 = 10^5$ integration periods. Assuming only a single detector, we limit arbitrarily the permitted bias in m^2 to be 0.06. From Eqs. (12) and (15) we get $U > 1.36\ \mathrm{m}^{-2/3}$. Similarly, we choose the permittable SNR to be 5 or $P/\mathrm{var}(P_0)^{1/2} = 5$. Now we obtain $U > 1.36\ \mathrm{m}^{-4/3}$. The matching stellar magnitude is[28]

$$m_v = \log_{2.51}(10^8AT_1\Delta\lambda\eta/U) = 8.14\text{–}2.5\log_{10}(U), \tag{17}$$

where we have substituted a detector area A of 0.002 m^2 (projected at the entrance aperture) and a bandwidth $\Delta\lambda$ of 300 nm. This high value is permitted for this wideband interferometer[1] in good seeing conditions; otherwise a much more restricted value is demanded.[11] An efficiency η of 0.015 is computed using an atmospheric transmission of 0.6, telescope reflectance of 0.6, optical efficiency of the interferometer and fibers of 0.8,

detector quantum efficiency of 0.1, and one image out of two. This last assumption is valid for many interferometers where one beam returns into the source.

The next step is to substitude the flux values derived from the demands for the minimal bias and SNR. We get

$$m_v = 7.81 + 5/3 \log_{10} \mathrm{m} \text{ (bias} < 3\%), \tag{18}$$

$$m_v = 7.81 + 10/3 \log_{10} \mathrm{m} \text{ (SNR} > 5). \tag{19}$$

With a lateral-shear interferometer, this is approximately the limit of the system at maximum shear, where we assume that only one detector is measuring. As the shear changes, the two-aperture images move and cross in front of the detectors. If we assume that the detectors cover the whole exit plane, the ratio of those measuring interfering light to those who do not is just the MTF of the system. With twenty parallel detectors functioning,[1] the limiting magnitude will be higher (or fainter) by 2.17.

Comparison with the results of others[5,11,29–32] is difficult, since specific values usually refer to a specific configuration of interferometer and detectors, and none applies to this case. Still they are all reasonably consistent with the above calculations.

E. Ribak is a Weizmann Fellow at Steward Observatory of the University of Arizona.

Appendix

We calculate the expectation values and variances of the various estimators serving to establish the modulus of the coherence function at each integration point. The underlying assumption is that the governing statistics are Poissonic. We start with the simple counter and go on to the sine and cosine ones. This straight counter measures the total flux falling on the detector during the measurement time (to be used as reference for the modulated signal) by adding the four quadrants

$$\begin{aligned} N = \langle N_0 \rangle &= K_2 \langle p_1 + p_2 + p_3 + p_4 \rangle \\ &= K_2(s_1 + s_2 + s_3 + s_4) \\ &= K_2 T_1 U = K_2 W = T_2 U, \end{aligned} \tag{A1}$$

where W is the average flux collected in a short integration time; here

$$\mathrm{var}(N) = \langle n_0 \rangle = N. \tag{A2}$$

The parallel calculation for the sine and cosine involves squares of differences and is not easy to do.[11] However, applying the powerful method of the moment-generating-function (mgf) simplifies it a great deal. Here we take advantage of the fact that the sine and cosine counter combinations are independent of each other. We calculate the expectation value and variance for each one of them separately and then add the results. We can alternatively write the expectation values in Eq. (7) as sums and differences of the terms $s = (T_1/4)2^{1/2} V \langle \sin\phi \rangle$, $c = (T_1/4)2^{1/2} V \langle \cos\phi \rangle$, and $b = (T_1/4)U$.

The mfg for p_1 will be

$$m_1(u) = \exp[(b + s)(e^u - 1)] \tag{A3}$$

and likewise for p_3

$$m_3(u) = \exp[(b - s)(e^u - 1)]. \tag{A4}$$

The mgf for $p_1 - p_3$ will be then

$$m_{13}(u) = m_1(u) m_3(-u) = \exp[(b + s)e^u + (b - s)e^{-u} - 2b]. \tag{A5}$$

The expectation value of $(p_1 - p_3)^2$ will be

$$m'_{13}(0) = 2b + 4s^2, \tag{A6}$$

and the variance

$$m^{(4)}(0) - [m'_{13}(0)]^2 = 8b^2 + 2b + 32s^2 b + 16s^2. \tag{A7}$$

For the other two terms we get similar results with c replacing s in the above equations. Now that we have the expectation value and variance for one cycle, we multiply by K_2 cycles and find for S_0

$$\begin{aligned} S = E(S_0) &= 4K_2(b + s^2 + c^2) \\ &= T_2 U(1 + Wm^2/2) = N(1 + Wm^2/2), \end{aligned} \tag{A8}$$

where we substituted a modulation term

$$m = (V/U)(\langle \sin\phi \rangle^2 + \langle \cos\phi \rangle^2)^{1/2}. \tag{A9}$$

Note that the bias in S was expected, since for Poisson statistics

$$\langle f^2 \rangle = \langle f \rangle^2 + \langle f \rangle. \tag{A10}$$

Similarly we get

$$\mathrm{var}(S_0) = N(1 + W + 2Wm^2 + W^2 m^2). \tag{A11}$$

References

1. E. Ribak, E. Leibowitz, and E. K. Hege, "Shearing Stellar Interferometer. 2: Optoelectronic Phase-Locked System," Appl. Opt. **24**, 3094 (1985).
2. M. Born and E. Wolf, *Principles of Optics* (Pergamon, London, 1976).
3. S. G. Lipson and H. Lipson, *Optical Physics* (Cambridge U. P., London, 1983).
4. A. Labeyrie, "High Resolution Techniques in Optical Astronomy," Prog. Opt. **13**, 49 (1976).
5. W. J. Tango and R. Q. Twiss, "Michelson Stellar Interferometry," Prog. Opt. **17**, 239 (1980).
6. F. Roddier, "The Effects of Atmospheric Turbulence in Optical Astronomy," Prog. Opt. **19**, 281 (1981).
7. R. H. T. Bates, "Astronomical Speckle Imaging," Phys. Rep. **90**, 203 (1982).
8. N. J. Woolf, "High Resolution Imaging from the Ground," Ann. Rev. Astron. Astrophys. **20**, 367 (1982).
9. J. C. Dainty, Ed., "Stellar Speckle Interferometry," in *Laser Speckle and Related Phenomena* (Springer-Verlag, New York, 1983).
10. C. Roddier and F. Roddier, "Fringe Visibility in a Michelson Interferometer," J. Opt. Soc. Am. **66**, 580 (1976).
11. J. J. Burke and J. B. Breckinridge, "Passive Imaging Through the Turbulent Atmosphere: Fundamental Limits on the Spatial Frequency Resolution of a Rotational Shearing Interferometer," J. Soc. Opt. Am. **68**, 67 (1978).

12. J. L. Elliot and I. S. Glass, "A Quantitative Fringe Detector for Stellar Interferometry," Astron. J. **75,** 1123 (1970).
13. W. S. Finsen, "Twenty Years of Double Star Interferometry and its Lessons," Astrophys. Space Sci. **11,** 13 (1971).
14. W. C. Wickes and R. H. Dicke, "An Automatic Interferometer for Double Star Observations," Astron. J. **78,** 757 (1973).
15. W. C. Wickes and R. H. Dicke, "Achromatic Double Star Interferometry," Astron. J. **79,** 1433 (1974).
16. D. G. Currie, "On the Amplitude Interferometer Program at the University of Maryland," IAU Colloquium 50, 7-1 (Maryland, 1978).
17. E. S. Kulagin, "A Superposed-Ray Interferometer," Sov. Astron. **13,** 1023 (1970).
18. D. Kelsall, "Optical "Seeing" Through the Atmosphere by an Interferometric Technique," J. Opt. Soc. Am. **63,** 1472 (1973).
19. J. C. Dainty and R. J. Scadden, "Measurement of the Atmospheric Transfer Function at Mauna Kea, Hawaii," Mon. Not. R. Astron. Soc. **170,** 519 (1975).
20. J. B. Breckinridge, "A Two-Dimensional White-Light Interferometer," IAU Colloquium 50, 31 (Maryland, 1978).
21. F. Roddier, "Rotation-Shearing Interferometry," IAU Colloquium 50, 32-1 (Maryland, 1978).
22. A. A. Tokovinin, "A Phase-Grating Stellar Interferometer," Sov. Astron. Lett. **4,** 229 (1979).
23. E. Ribak and S. G. Lipson, "Complex Spatial Coherence Function: Its Measurement by Means of a Phase-Modulated Shearing Interferometer," Appl. Opt. **20,** 1102 (1981).
24. M. Dugan, "Shearing Interferometer for the Measurement of Atmospheric MTF, M. Sc. Thesis, U. Rochester, New York (1982).
25. C. J. Oliver and E. R. Pike, "Statistical Accuracy in the Photon Counting Structure Function of Fluctuating Light Fields," Opt. Acta **28,** 1345 (1981).
26. K. Schatzel, "Noise in Photon Correlation and Photon Structure Function," Opt. Acta **30,** 155 (1983).
27. A. A. Tokovinin, "The Influence of Turbulence on the Operation of a Stellar Interferometer," Sov. Astron. Lett. **6,** 386 (1980).
28. C. W. Allen, *Astrophysical Quantities* (Clowes, London, 1972), p. 197.
29. S. M. Kozel, "On the Fluctuation Resolution Limit of an Optical Modulation Interferometer," Sov. Phys. JETP **5,** 609 (1957).
30. D. V. Korolkov and O. I. Krat, "On the Sensitivity of a Stellar Interferometer with Incoherent Accumulation of the Signal," Sov. Astron. **20,** 370 (1976).
31. A. H. Greenaway and J. C. Dainty, "The Formal Equivalence Between Autocorrelation and Power Spectra Analysis of Photon-Limited Data," Opt. Commun. **35,** 307 (1980).
32. K. Itoh and Y. Ohtsuka, "Photon-Noise Limitations in Wave-Front-Folding Interferometry," J. Opt. Soc. Am. **73,** 479 (1983).

Shearing stellar interferometer. 2: Optoelectronic phase-locked system

Erez Ribak, Elia Leibowitz, and E. Keith Hege

A parellel-shear interferometer was built which is able to provide the visibility of celestial objects in real time in the presence of atmospheric turbulence. The interferometer consists of two beam splitters and a modulating/shearing element and is stable and efficient. At each shear value the fringes have constant visibility, but their atmospheric-induced phase is random in time and space. A water cell modulates the optical path at a frequency above that of most atmospheric fluctuations. The modulated interference pattern is transferred via fiber optics to a bank of photomultipliers off the telescope. A set of digital lock-in amplifiers and a microprocessor give the (incoherent) sum of the fringe visibilities every few milliseconds. First observations show the promise of the technique and reveal needed refinements.

I. Introduction

High resolution astronomy is greatly assisted today by speckle interferometry. Using standard optical and electronic instrumentation, this method serves to acquire the autocorrelation function of celestial objects and is progressing toward obtaining a full image reconstruction. A problem with speckle interferometry is that a great deal of data processing must be done before results appear.

Another method, namely, shearing interferometry, can be applied which can retrieve the same results. A lateral-shear interferometer, which utilizes optical and digital parallel processing in real time, can provide particular subsets of the image amplitude at will. The price is more complicated optics and specialized electronics and the need to scan serially the image plane to acquire the full autocorrelation.

We have built a parallel-shear interferometer, which includes a novel detection system. The reason for this choice and a comparison between various interferometers are given in a parallel paper.[1] Also discussed there is the rationale and detailed analysis of the digital data processing detection scheme employed as well as the limiting SNR for faint object observation. We here describe the combined system and try to assess its performance.

II. Optical System

Development of the optical system began as a simulation in the laboratory on an optical bench, which included also some atmospheric effects.[2] The basic structure (Fig. 1) is similar to that of a Twyman-Green interferometer. The interferometer is made of two cube beam splitters, one splitting the light into two beams, the other recombing them. Each beam can be reflected only once per element; the separation is achieved by refraction in the same beam splitter. This halves the number of elements to two, thereby reducing the number of adjustments. The parallellism of the beams also nearly eliminates the sensitivity to vibration. Since the beam splitters are neither ideal nor equal, the amplitudes of the beams are polarization and wavelength dependent. This makes one pair nonsymmetric, reducing its interferometric contrast by ~40–60%.

Atmospheric turbulence randomly changes the fringe phase but not the contrast. In this work we chose to measure this contrast by internally modulating the fringes at a relatively fast rate during a period within which the atmosphere can still be assumed to be stagnant (usually a few milliseconds). This integration period should include as many modulation cylces (or as high a frequency) as possible to have a minimal relative bandwidth. Electronic considerations, however, limit the frequency to below 1 MHz, since the dead time of the system goes up linearly with frequency. (This dead time is due mostly to the photon counters not being able to register while switching direction.)

E. Keith Hege is with University of Arizona, Steward Observatory, Tucson, Arizona 85721; the other authors are with Tel Aviv University, Physics & Astronomy Department, Ramat Aviv, Tel Aviv 69978, Israel.

Received 27 October 1984.
0003-6935/85/183094-07$02.00/0.

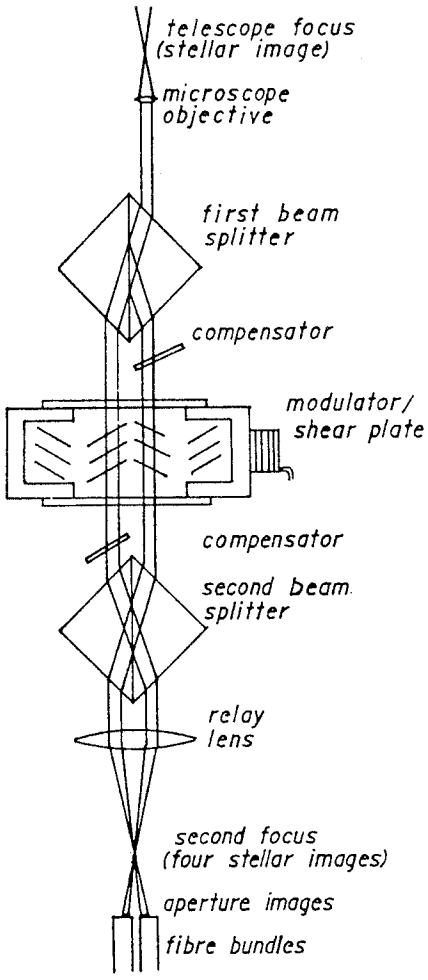

Fig. 1. Optical layout of the interferometer. The element between the dividing and recombining beam splitters is a water cell serving both for modulation and shear.

A search has been conducted for a suitable modulator fulfilling the following demands: (a) the given frequency range; (b) phase (path length) modulation on parallel rays; (c) insensitivity to the polarization of the (star)light; (d) ease of drive (low voltage, low power); and, if possible, (e) low price. The device used in the simulation, namely, a wobbling glass plate in one path, could not be adopted as it was too slow. Electrooptic modulators were also ruled out since they consume at least half of the light by using polarizers. A rotating glass disk of variable thickness, which the two beams cross on the perimeter, was found to be too difficult to manufacture.

The solution which was adopted answers most of these demands.[3] It is a simple water cell which the two parallel beams traverse. A density (bulk) wave is introduced into the water and across the beams by an external piezoelectric element (usually a ceramic stack). As the local density of the water changes, so do the effective path lengths of the two beams, in an inverse oscillatory manner. To minimize the power needed to drive the modulator, the system is tuned to produce a standing wave, which the two beams traverse at opposite (out-of-phase) antinodes.

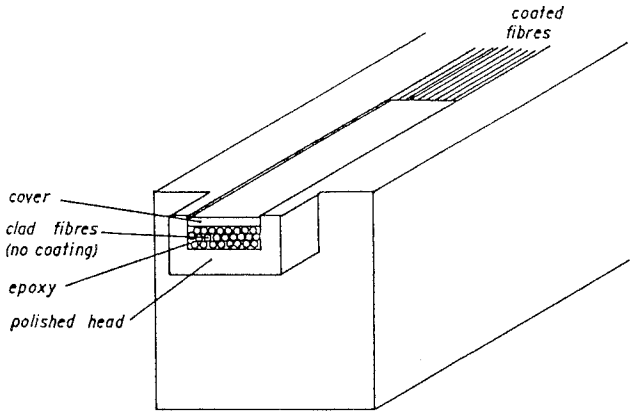

Fig. 2. Fiber bundle head. After the fibers were glued in, the bundle and head were polished as one unit.

The limitations of this water modulator are (a) limited efficiency of ~70% due to the sinusoidal (rather than linear) path changes, (b) frequency doubling produced by this nonlinearity for too high an amplitude, (c) resonance has to be wide (low Q) or it is hard to maintain, and (d) the demand that the beams pass through opposite nodes places some restrictions on either the beam separation or the modulation frequency. Convenient values were found to be in the 80–120-kHz range.

The other function of this modulator element is to shear the beams. Rotating it slightly shifts the two rays parallel to themselves so as to produce the desired shear after leaving the second beam splitter.[2] A rotation of up to 30° (each way) for large images can be achieved by a stepping motor and a cam.

The interferometer includes only plane surfaces. Therefore, the beams must be collimated when traversing it; otherwise the fringe spacing will vary with the shear. The diameter of the beam going through the interferometer must be small to accommodate the limited system aperture. Finally the entrance aperture has to be reimaged on the detection plane in the appropriate demagnification. These demands lead to the following structure: one lens (a microscope objective), immediately following the telescope focus and sharing the same focal plane, forms a collimated beam. Typically the diameter of this beam is 1–3 mm. After passing through the interferometer (the length of which is 30 cm), another relay lens (of 10-cm focal length) reimages the entrance aperture onto the detection plane without further magnification. A sliding mirror and an independently sliding eyepiece enable one to view either one or both images.

The two interfering pupil images are transmitted via two fiber bundles, each containing some thirty silica fibers. The bundle heads have a rectangular shape of 1200 × 500 μm. The fibers, protective coat removed, are organized in a close-packed matrix of three rows (Fig. 2). The core-to-cladding ratio of the fibers is 100/140 μm, leading to some 50% of the light incident on the cores. The rest of the light is not necessarily lost, since modes advancing in the cladding can also reach

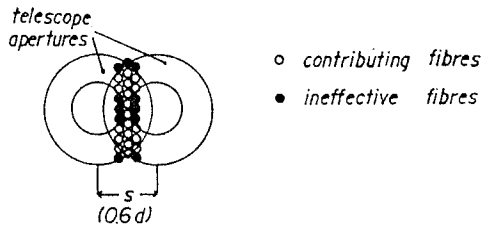

Fig. 3. Measuring array: only fibers in the overlap area are effective; the others contribute to the background signal.

the other end of the fibers, 6 m away. The fiber heads are mounted on small x-y tables adjustable by millimetric screws.

The demands on the mechanical structure of the interferometer were quite restricting. First, a rigid holder to carry the entire optical structure was obligatory. Easy alignment demanded that the optical elements be able to move sideways as well as rotate around their centers with both motions totally independent. This was solved by putting them on small rotating platforms, riding on tables which slide with respect to the base. All elements were machined of aluminum to reduce weight.

Then there was the need for the whole interferometer to rotate around the telescope optical axis to measure objects at different orientations. For this purpose an iron tube containing the collimator lens was connected to the telescope bottom. The flat base of the interferometer was then fastened to this tube by means of two iron V-holders which ensure exact rotation about the center axis. As a result of this structure, the pointing error of the aligned system for two different orientations is <1 sec of arc.

III. Electronic System

This is the other main element of the interferometer and the one which makes it a practical device. It consists of twenty channels, each beginning with fiber optics leading into a photomultiplier, followed by a preamplifier, the latter feeding two digital lock-in counters and a straight photon counter. All the counters are read by a central microcomputer which also handles the data processing as well as determines the integration times and changes the shear by moving the stepping motor.

The feasibility study was done in two stages. First, an analog lock-in amplifier was tried, but its low frequency response and price prohibited using it in a multiple system. (The cost of components for the final integrated system described here was <$2000.) In the next stage a single digital channel was built containing two quadrature lock-in detectors and a simple flux counter to find the fringe contrast.[1] This instrument was insufficient, since light cannot not fall at all shearing steps on a single detector; a multiple system had to be built with different detectors responding at different stages of shear (see Sec. V and Fig. 3). Thus a twenty-channel real-time readout system was devised and built at the Wise Observatory, Tel Aviv University (Fig. 4). It consists of five main blocks: photodetectors;

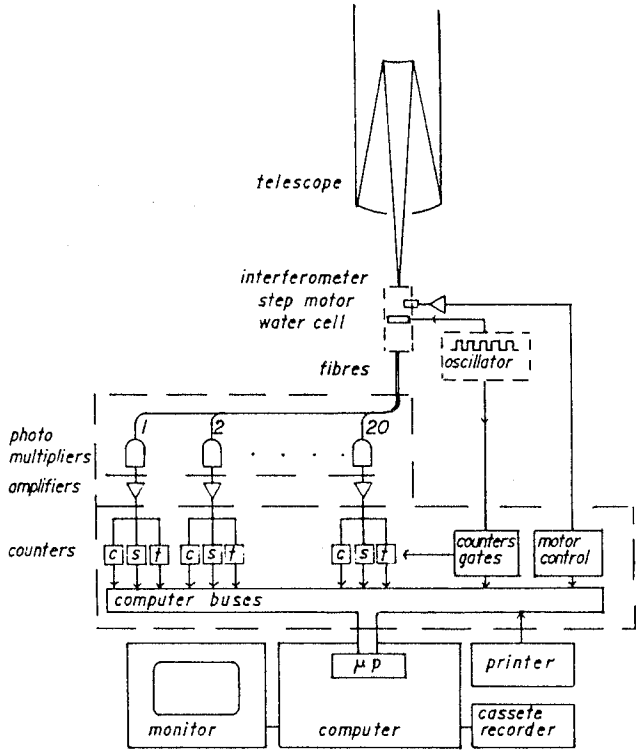

Fig. 4. Main units of the electronic system are (from top) oscillator (for lock-in reference and to drive the modulator), detectors, preamplifiers, lock-in counters (including step motor and counters controls), and computer for running the system and processing data.

preamplifiers; phase-locked counters; modulator driver; and computer.

First there are twenty photomultipliers, each fed by three fibers from different places in the two interferometer output pupils. Referring again to Fig. 3, we notice that interference occurs at the overlap area of the two pupil images. As the shear changes, this overlap area changes shape, rendering different fibers ineffective. If we can smartly combine fibers from various points into one detector, at any shear step only one fiber will be effective, and the other two will see either one (noninterfering) image or none at all.

The tubes (RCA 931B) are side-on, blue-sensitive, and moderately good for photon counting. Their choice was made because of their relatively low dark current (but primarily for their low price). A severe drawback is that they have quite differing sensitivity and threshold. This is partly overcome by feeding all tubes by one internal high voltage source, each through different load resistors to equalize their responses at the working voltage, 1 kV.

The weak photoelectron signals of the tubes are led by short coaxial cables (2–8 cm) to twenty preamplifiers sharing the same box. These constitute the second block. They are monolithic chips (LeCroy MVL-100)[4] which produce a standard ECL pulse above some determinable threshold. They are mounted on four standard printed-circuit boards next to the tubes and share a common power supply. The design is similar to that of DuPuy.[5]

The twenty outputs of the preamplifiers then plug through short (20-cm) coax cables into the lock-in counters. These come in a different box, whose hinged cover is the photomultipliers–preamplifiers box. One of the problems associated with this structure is that the incoming and outgoing coaxes have to be screened from each other to avoid oscillations of the preamplifier. A diagnostic subroutine before observations always makes sure this does not happen. This is done by looking separately at each preamplifier output at very low light levels and verifying that double (or multiple) events to not occur.

Now comes the third block, which demanded most of the engineering. It includes twenty square-law detectors, each placed on a different card. The purpose of each detector is to capture the squared amplitude of the modulation, which calls for two phase-sensitive detectors in quadrature and a simple flux accumulator.[1] First, the positive part of the ECL signal is conditioned into a standard TTL signal. It is then fed into either one of the two up–down counters as well as into the straight counter. Each up–down counter is assigned pulses for a quarter cycle, then stops for one quarter, during which it flips its direction, then counts for the next quarter cycle, and finally stops for the last quarter and flips direction again (Fig. 5). The other up–down counter is in quadrature with this counter, and it would count while the other does not, then stop, and flip while the other counts. A third, up-only counter, acquires the simple flux of photons.

At the end of the integration all pulses are inhibited, and the contents of the counters are moved to three latches for the computer CPU to read on its own time. Then the counters are reset back to zero, and counting resumes. This happens simultaneously on all sixty counters, as the timing signals fed into them are the same.

The counters are all 8-bit units, which means that the sine/cosine ones are limited between the 127 and −128 values, and the straight (up-only) counter can read up to 255. If the rates are higher, the result is wrong, without possibly knowing about it. Using the diagnostic subroutine mentioned above to look at the counter outputs at a high light level might reveal this, since the signal will fluctuate wildly between zero and 255. There are two steps that can be taken against this: lower the light level artificially by using filters or shorten the integration time.

Two additional cards perform instrument control tasks. One serves as a demultiplexer for addressing the various counter latches and as a controller for the stepping motor. The other one is the time card, on which are formed all the necessary gating functions needed to start, read, or reset the sine, cosine, and straight counters on the twenty adjacent cards. The clocking for these is provided by the water-cell modulator.

As described above, the interference fringes are modulated in a water cell by a piezoelectric driver. This element requires a special voltage supply (70-V P–P at 100 kHz). It is desirable that this power supply be close

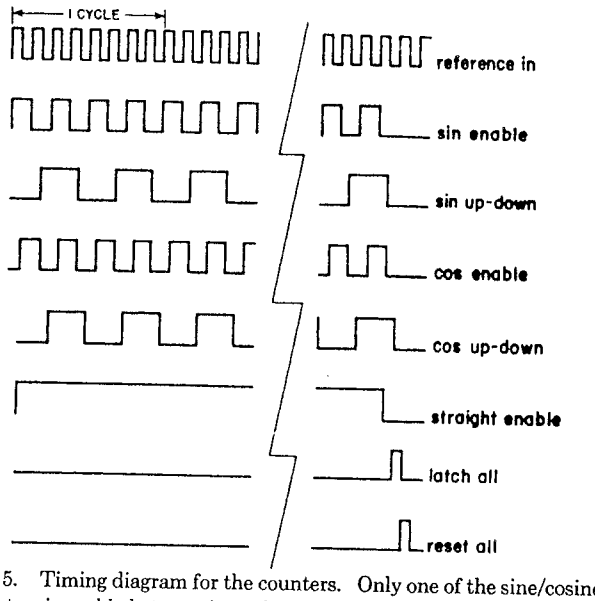

Fig. 5. Timing diagram for the counters. Only one of the sine/cosine counters is enabled at any time. Pulses are fed into either one of these as well as into the flux counter. The first two flip direction when not active.

to the driver and not to the photomultiplier/preamplifier electroncs so as to reduce spurious electromagnetic coupling. Another advantage of this proximity is that the observer can adjust the frequency and amplitude while looking at the modulated fringes. Thus the power supply was built as a separate box and mounted on the telescope. Essentially it contains a variable oscillator at ~1 MHz, whose frequency is divided by eight and amplified for the piezoelectric driver. The same 1-MHz signal is transferred to the lock-in detectors timing card.

The fifth block is the microcomputer. The computer utilized in the data collection is a Z80-based home computer, the Timex Sinclair 2068 (64K memory). A direct connection is made to the data bus lines and top eight address lines in conjunction with the IN/OUT command (available also in BASIC). This system features down-counting to zero which is readily available on these top eight address lines. The computer is connected to a monitor and a simple tape recorder for program storage and data logging. As the rate of accumulated data is low, a faster recording medium, such as a diskette unit, is not required. Specifically, saving any amount of data and verifying it take ~3 min, which is almost irrelevant compared to the total measurement time.

IV. Computer Program

Special tape-loaded programs and subroutines were developed for instrument control, data collection, and on-line reduction. A diagnostic subroutine (written in Z80 assembler language) lets the counters accumulate for one integration cycle, then loads the sixty results into memory. The program in BASIC displays them on the screen including the depth of modulation for each of the twenty channels. This is done by squaring the sine and the cosine, adding them, and subtracting the straight (or intensity) counter of this channel.

The purpose of the second assembler coded subroutine SQUAD is to collect, square, and add the results from the twenty channels as fast as possible according to the scheme discussed in the parallel paper[1] (Fig. 6). It first sets the short integration time, at the end of which all the counters move their contents to the latches, and a flag is raised. The program goes on to read the first sine counter. It uses a look-up table to get the absolute value of the reading, then another table to read the square of this value. The square is then added to one memory cell. Then the process is repeated for the cosine counter, and its square is also added to the same cell. Last, the straight counter is read, and its value is added to a second cell. The process is repeated twenty times, and all the results are added to the *same two cells.* The program keeps doing so for a precalculated number of cycles (the long integration time) and returns to BASIC the contents of these two cells. It should be emphasized that while collection and reduction are done, the counters keep accumulating for the next cycle. The shortest integration time possible is 2.3 msec.

V. System Operation and Evaluation

A brief description of the interferometer alignment and operation is given followed by its evaluation. With a strong star at the center of the telescope field, the first lens is secured right behind the telescope focus producing a collimated beam. Than the two beam splitters are adjusted in place, ensuring that the four beams are parallel to each other. This is done by adding in the second lens and eyepiece and verifying that the four star images (Fig. 1) coincide. The modulating cell and the two compensating plates are put into place, and a search is made for an equal path (white light fringe). Sometimes, and only with strong sources, it helps if one uses a medium-band filter to increase the tolerance (see below).

After finding the fringes, there are generally three minor errors to be corrected: (a) Nonparallel beams through the interferometer, which lead to a movement of the fringes across the image while shearing. This can be corrected by slightly rotating the beam splitters. Care should be taken as this can happen because the star has tracked out of the center of the field. That can be verified by rotating the interferometer around the telescope axis, which should not affect the picture. A quide star might come in handy. (b) Crowding (changing density) of the fringes while shearing which can be attributed to a noncollimated ray at the interferometer input. The cure is a refocusing of the telescope. (c) A white fringe off-center, caused by nonequal paths of the two beams, which can be adjusted into place by the compensating plate.

The fiber optics must be accurately placed at the output pupil plane. Unfourtunately, the asymmetric image does not contribute to the signal significantly, and, therefore, there is not much use for the corresponding fiber head. A coarse setting of the modulator driver is made by looking for a resonance frequency at which the fringes are smeared (at least for the human eye). Data collection can then be done.

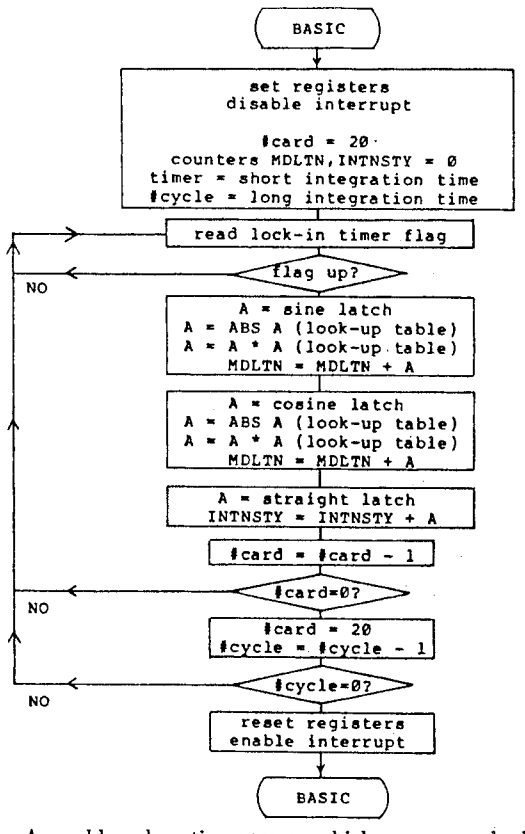

Fig. 6. Assembly subroutine SQUAD, which squares and adds all twenty channels. A single cycle takes <2.3 msec.

When starting observation, the main BASIC program first calls the diagnostic subroutine for setting of the integration time. The shear motor is moved automatically to its initial position (usually at maximum shear), and it starts collecting data by calling SQUAD. When finished, it prints on-screen the results for the first shear value, then proceeds to the next position. At the end of the observation the visibility, as a function of shear, is displayed graphically. The raw data are recorded on tape and printed on paper.

After describing the interferometer, here are its weaker points (and suggested solutions). Unfortunately, most are common to many high resolution systems. The first one is sensitivity to wave front tilt. Such a tilt can be caused by either bad tracking or atmospheric turbulence (although the latter decreases at low spatial frequencies). A 1-sec of arc error amounts to a total of 5 μm over a 1-m aperture or twenty (yellow light) fringes. The effect is twofold, as it results in a partial disappearance of fringes, combined with reduction in the demodulated signal due to the frequency change caused by the movement.

The bandwidth of the system is set by the optical elements and the photomultipliers to be ~300 nm, and the number of fringes is ~20. To overcome the tilt and track errors, it will have to be reduced to ~100 nm. The loss of light will mean worse SNR, but can be compensated somewhat by using dichroic mirrors and observing at a few wavebands simultaneously. A second solution is to use some of the light of the star (either from the

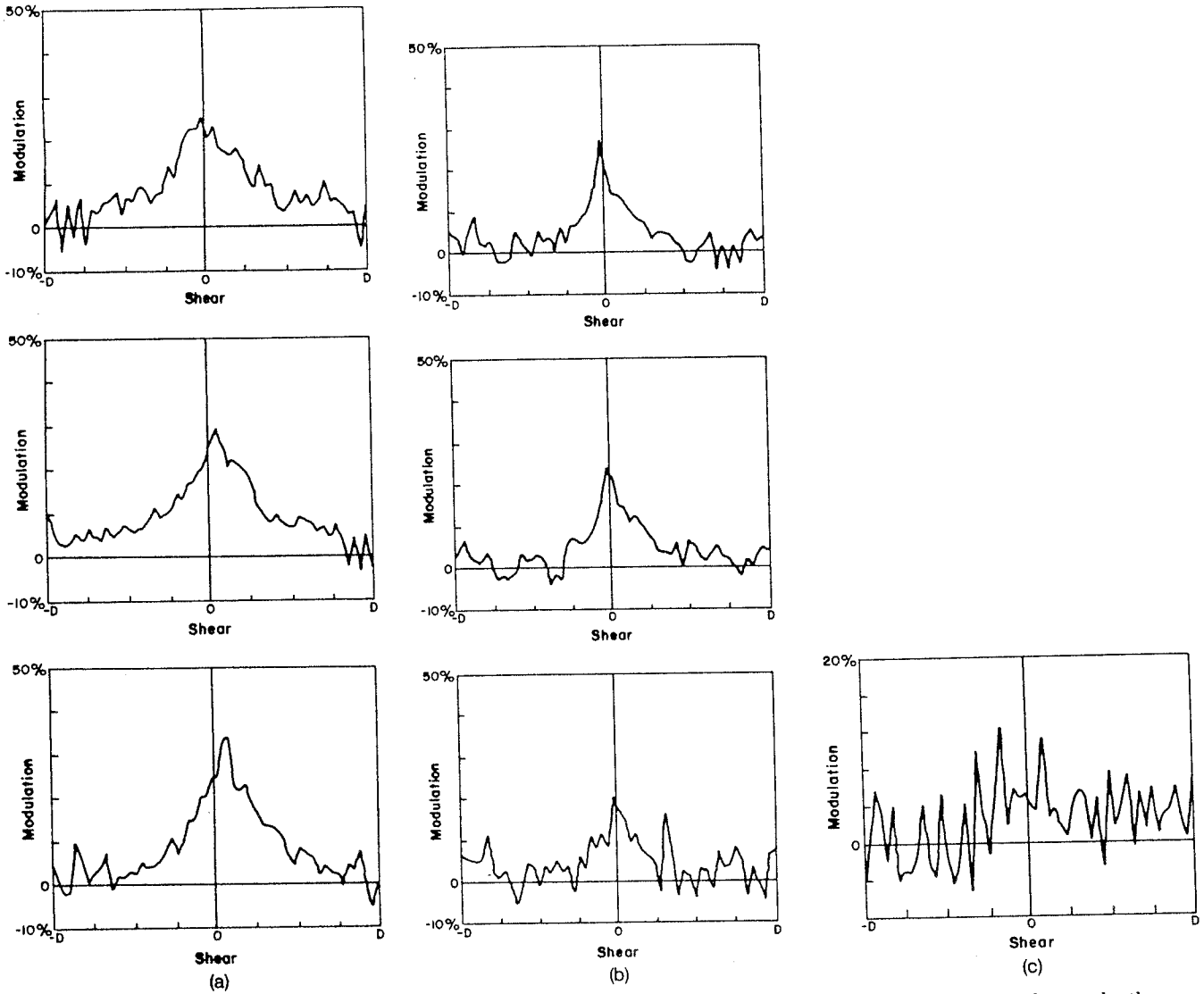

Fig. 7. Consecutive interferograms (percent modulation as a function of shear) of (a) Spica, (b) Antares, and (c) ϕ Dra, done under the same conditions: 25-msec short integration time; 10-sec dwell time per shear value (spatial frequency); 55 shear points (27 on each side; D is the telescope diameter, 238 cm).

asymmetric image or diverted by a dichroic mirror as above) to guide on and correct the first-order tilt.

Another problem is that of coupling the light from the interference pattern into the detectors. Apart from the limited efficiency, the drawbacks are the sensitivity to position and size and use of nonrelevant detectors. The sensitivity to position means that the fiber bundle (or any detector) has to be positioned accurately (within $\sim$30 μm) relative to the image of the sheared apertures. The second problem is scale. The size of the fibers is fixed, but that of the atmospheric isoplanatic patch is not, so one is limited to one scale, dictated at the beginning of the observation by the ratio of the aperture image to the fibers. A zoom apparatus, which will magnify or demagnify the whole aperture without loosing too much light, could be used.

And the third most severe problem is that of inefficient imaging. As the apertures shear across one another, some detectors see areas that are not overlapping and hence reduce the effective fringe contrast (Fig. 3). As the system stands now, it does not care to distinguish between the different channels (as they should all yield the same information). A solution is to have each detector measure only when it has fringes appearing. This will call for an exact position calibration at the expense of data collection rate, which seems worth it.

VI. Data Collection and Reduction

The performance of the interferometer was assessed on two telescopes: the Wise observatory 1-m telescope in Israel and the Steward observatory 2.28-m telescope on Kitt Peak, Tucson, Ariz. We report here an observation using the latter on 20–22 Mar. 1984. Seven measurements were taken with careful guiding of the telescope under 1.4-sec of arc seeing conditions. The tolerance was relieved further by using a 20-nm bandpass filter centered around 500 nm, which ensured that

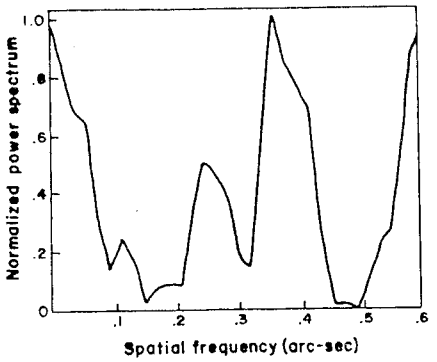

Fig. 8. Power spectrum of the squared fringe visibility of ϕ Dra [Fig. 7(c)]. The main component is at 0.38 sec of arc.

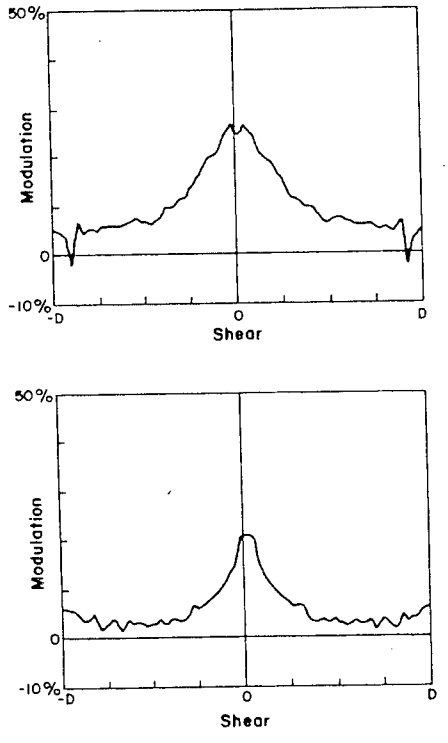

Fig. 9. Average of the Spica interferograms (top) achieved by summing both left and right components of three interferograms [Fig. 7(a)] and of Antares (bottom) averaged from Fig. 7(b).

fringes stay in the overlap area for even the highest wave front tilt.

All measurements were taken under the same internal conditions: modulation frequency of 80.5 kHz; short integration time of 25 msec; long integration time of 10 sec; and 55 shear points (maximum-zero-maximum shear) totaling 550 sec. The direction was always east–west, and the objects were α Vir (Spica), α Sco (Antares), and ϕ Dra. Unfortunately, the last one was taken as the sun was rising, and the data are unreliable. Spica and Antares were quite low (~30–40° zenith angle).

All the data show the same features (Fig. 7), Poisson noise and atmospheric fluctuations allowed for, and clearly the Spica curves are much wider (or sloping slower to zero) than the Antares ones. The ϕ Dra data show some modulation, at least on the left-hand side, before the solar light interference became too high. Fourier analysis made on the latter (Fig. 8) shows a component at 0.38 ± 0.11 sec of arc (reflected in the east–west direction). The uncertainty is rather high, as it relies on too little data. This 4.22^m star has a component 1.7^m darker at a separation of 0.311 sec of arc, position angle 280° (1981 values[6]).

The Spica data were treated as follows. First, the three sets were folded around the center (zero shear), then added together, as if into one run with six times the (long) integration time. This meant that the raw data with plus and minus the same shear value of all three interferograms were combined. The same procedure was applied to Antares (Fig. 9). The results show that the visibility function of Antares is narrower than that of Spica. The two visibility functions were deconvolved by divisioin in the Fourier plane producing a very noisy result. To find the approximate diameter of the star, a uniform disk model was fit to the deconvolved function. Linear regression to the data was done under the assumption that either the errors increased with shear or were constant. The results correspond to 33 ± 7 or 44 ± 6 msec of arc. Evans[7] has measured the star by occultation methods and found its diameter to be 41 ± 1, and Currie *et al.*[8] used amplitude interferometry to determine the value of 42 ± 5. The reference star can be considered a point source, as its diameter is <1 msec of arc.[9]

Special thanks to Peter Ibbetson of the Wise observatory for help in planning and building the electronic part. E. Ribak is on a Weizmann fellowship at Steward Observatory of the University of Arizona.

References

1. E. Ribak and E. Leibowitz, "Shearing Parallel Interferomter. 1: Digital Data Analysis Scheme," Appl. Opt. **24**, 3088 (1985).
2. E. Ribak and S. G. Lipson, "Complex Spatial Coherence Function: Its Measurement by Means of a Phase-Modulated Shearing Interferometer," Appl. Opt. **20**, 1102 (1981).
3. E. Ribak and E. Gazit, "Simple Nonpolarizing High-Frequency Modulator for Interferometry," J. Phys. E **14**, 701 (1981).
4. High Energy Physics Division, LeCroy Research Systems Corp., 700 S. Main Street, Spring Valley, N.Y. 10977.
5. D. L. DuPuy, "An Integrated Circuit Pulse Amplifier for Use with Photomultipliers," Pub. Astron. Soc. Pac. **93**, 144 (1981).
6. H. A. McAlister and W. I. Hartkopft, Catalog of interferometric measurements of binary stars, Georgia State U. (1984).
7. D. S. Evans, "Antares: a Discussion of the Observations," Astron. J. **63**, 83 (1957).
8. D. G. Currie, S. L. Knapp, K. M. Liewar, and R. H. Braunstein, U. Maryland Technical Report 76-125 (1976).
9. R. Hanbury-Brown, *The Intensity Interferometer* (Taylor & Franics, London, 1974).